Do Emergent Constraints on Carbon Cycle Feedbacks Hold in CMIP6?

Sabrina Zechlau[1,2] [ID], **Manuel Schlund[1]** [ID], **Peter M. Cox[3], Pierre Friedlingstein[3,4], and Veronika Eyring[1,5]** [ID]

[1]Deutsches Zentrum für Luft- und Raumfahrt e.V. (DLR), Institut für Physik der Atmosphäre, Oberpfaffenhofen, Germany, [2]Meteorologisches Institut, Ludwig-Maximilians-Universität, Munich, Germany, [3]College of Engineering, Mathematics and Physical Sciences, University of Exeter, Exeter, UK, [4]LMD/IPSL, ENS, PSL Université, Ecole Polytechnique, Institut Polytechnique de Paris, Sorbonne Université, CNRS, Paris, France, [5]Institute of Environmental Physics (IUP), University of Bremen, Bremen, Germany

Abstract Emergent constraints on carbon cycle feedbacks in response to warming and increasing atmospheric CO_2 concentration have previously been identified in Earth system models participating in the Coupled Model Intercomparison Project (CMIP) Phase 5. Here, we examine whether two of these emergent constraints also hold for CMIP6. The spread of the sensitivity of tropical land carbon uptake to tropical warming in an idealized simulation with a 1% per year increase of atmospheric CO_2 shows only a slight decrease in CMIP6 (−52 ± 35 GtC/K) compared to CMIP5 (−49 ± 40 GtC/K). For both model generations, the observed interannual variability in the growth rate of atmospheric CO_2 yields a consistent emergent constraint on the sensitivity of tropical land carbon uptake with a constrained range of −37 ± 14 GtC/K for the combined ensemble (i.e., a reduction of ~30% in the best estimate and 60% in the uncertainty range relative to the multimodel mean of the combined ensemble). A further emergent constraint is based on a relationship between CO_2 fertilization and the historical increase in the CO_2 seasonal cycle amplitude in high latitudes. However, this emergent constraint is not evident in CMIP6. This is in part because the historical increase in the amplitude of the CO_2 seasonal cycle is more accurately simulated in CMIP6, such that the models are all now close to the observational constraint.

Plain Language Summary The statistical model of so-called emergent constraints help to better understand the sensitivity of Earth system processes in a changing climate. Here, we analyze the robustness of two previously found emergent constraints on carbon cycle feedbacks, using models from the Coupled Model Intercomparison Project (CMIP) of Phases 5 and 6. First the decrease of carbon storage in the tropics due to increasing near-surface air temperatures, which is found to be robust on the choise of model ensemble. Giving a constraint estimate of −52 ± 35 GtC/K for CMIP6 models, being within the range of uncertainty for the previously estimated result for CMIP5. Second, the increase of carbon storage in high latitudes due to CO_2 fertilization effect, which is found to be not evident among CMIP6 models. This is in part because the historical increase in the amplitude of the CO_2 seasonal cycle is more accurately simulated in CMIP6, such that the models are all now close to the observational constraint.

1. Introduction

The carbon cycle plays a major role in how climate evolves in the future. Carbon dioxide (CO_2) emissions from fossil fuel burning and from land use change increase the amount of CO_2 in the atmosphere, which is the main driver of the observed anthropogenic warming since preindustrial times due to its radiative effect as a greenhouse gas (Masson-Delmotte et al., 2022). Changes in temperature and in atmospheric CO_2 concentration lead to changes in the carbon cycle, thus forming important Earth system feedbacks (Friedlingstein et al., 2006). First, the carbon-concentration feedback constitutes a negative feedback since enhanced levels of atmospheric CO_2 concentration increase plant photosynthesis. As a result, more carbon is removed from the atmosphere and stored in vegetation and soils. However, this land carbon sink is reduced by the second feedback of the carbon cycle. The carbon-climate feedback constitutes a positive feedback, since increasing temperatures reduce plant productivity in most regions and increase soil organic matter decomposition, thus reducing the terrestrial carbon sink. As a result of this positive feedback, more carbon stays in the atmosphere which leads to further warming (Cox et al., 2000; Friedlingstein et al., 2001, 2006). Mathematically, the response of the Earth's carbon cycle can be

characterized in terms of the carbon-climate feedback parameter γ and the carbon-concentration feedback parameter β, which quantify the change in terrestrial carbon reservoirs in response to climate warming and increases in atmospheric CO_2 concentration, respectively (Friedlingstein et al., 2003; Gillett et al., 2013).

Earth system models (ESMs) with interactive carbon cycle are able to simulate these feedbacks (Jones et al., 2016). However, ESMs participating in the Coupled Model Intercomparison Project Phase 5 (CMIP5; Taylor et al., 2012) simulate a wide spread in global land carbon storage (Arora et al., 2013a, 2013b). Furthermore, Arora et al. (2013a, 2013b) diagnosed a large spread in global carbon cycle-climate (-21.3 to -88.6 GtC/K) and carbon cycle-concentration (0.22–1.46 GtC ppm^{-1}) feedback parameters in these same models. In the more recent CMIP Phase 6 (CMIP6; Eyring et al., 2016a), the size of the terrestrial carbon sink remains one of the key unknowns in ESMs with interactive carbon cycle (Arora et al., 2020). Reducing uncertainties in carbon cycle feedbacks therefore remains a priority in climate modeling.

Emergent constraints are a promising method to constrain uncertainties in Earth system feedbacks with present-day observations (Eyring et al., 2019). This method is based on relationships across an ensemble of models between some aspect of an unobservable Earth system sensitivity and an observable trend or variation in the current climate.

An observationally based constraint on the carbon-climate feedbacks was first published by Cox et al. (2013). They found that the global mean growth rate of atmospheric CO_2 concentration is strongly correlated with the tropical near-surface air temperature on interannual time scales, mainly caused by the El Nino Southern Oscillation (ENSO) variability originating from the Tropical Pacific Ocean. This correlation describes the same effect of temperature on terrestrial carbon storage in the tropics on a short and observable time horizon as on the long centennial time scale as diagnosed in the land carbon-climate feedback. Cox et al. (2013) found the feedback parameter to be about -53 ± 17 GtC/K. This emergent constraint was confirmed by Wenzel et al. (2014) (hereafter W14), who used an ensemble of eight CMIP5 models. Using a slightly different method to diagnose the observed interannual variability (IAV) of CO_2 to tropical near-surface air temperatures ($\gamma_{IAV} = -4.9 \pm 0.9$ GtC/yr/K) they could constrain the carbon cycle-climate feedback parameter to -44 ± 14 GtC/K.

An emergent constraint on the carbon-concentration feedback in the CMIP5 ensemble was published by Wenzel et al. (2016) (hereafter W16). The authors assumed that an atmospheric CO_2-driven increase in GPP, as simulated in future scenarios, would be accompanied by an increase in the observed seasonal amplitude of the atmospheric CO_2. They indeed found the fractional change of Gross Primary Productivity (GPP) for a doubling of atmospheric CO_2 to be well-correlated with the increase in the atmospheric CO_2 amplitude measured at midlatitude and high latitude. Observational data were therefore able to narrow the estimates for the relative GPP increase under a doubling of atmospheric CO_2 concentrations, to $37 \pm 9\%$ for high-latitude ecosystems, and $32 \pm 9\%$ for extratropical ecosystems.

However, the absolute values of the feedback parameters are known to be sensitive to the chosen model ensemble, the simulation scenario, and the mathematical framework (Boer & Arora, 2009; Gregory et al., 2009; Hajima et al., 2014; Zickfeld et al., 2011), hence also affecting the emergent relationship. Therefore, it is crucial to investigate previously derived emergent relationships *out-of-sample* on new model ensembles, such as CMIP6.

In this study, we examine whether the previously published emergent constraints on these two carbon cycle feedbacks, originally reported for the CMIP5 ensemble, still hold for the CMIP6 ensemble. We adopt identical methods to diagnose the present-day diagnostics and the carbon cycle feedbacks, as described in Section 2. The updated emergent constraints on carbon cycle feedbacks are then presented and discussed in Section 3 and summarized in Section 4.

2. Data and Methods

2.1. Models and Model Simulations

In order to test the emergent constraints out-of-sample with a new ensemble that was not included in the original studies (W14, W16), we use ESMs with an interactive carbon cycle that participate in CMIP6 (Eyring et al., 2016b), which are in particular models from the Coupled Climate-Carbon Cycle Model Intercomparison Project (C4MIP; Jones et al., 2016). The consistent CMIP experimental design additionally allows us to combine the previous CMIP5 models with the CMIP6 models to form a larger ensemble of models. This helps to test the

Table 1
Overview of CMIP5 and CMIP6 Models Included in This Study

Ensemble	ESM	Land modules	Ocean modules	Nitrogen cycle	EC on γ/β	Main reference
CMIP5	CanESM2	CLASS2.7 and CTEM1	CMOC	No	$\gamma + \beta$	Arora et al. (2011)
	CESM1-BGC	CLM4	BEC	Yes	$\gamma + \beta$	Gent et al. (2011) and Lindsay et al. (2014)
	GFDL-ESM2M	LM3	MOM4	No	$\gamma + \beta$	Dunne et al. (2012)
	HadGEM-ES	JULES and TRIFFID	Diat-HadOCC	No	γ	Clark et al. (2011) and Cox (2001)
	IPSL-CM5A-R	ORCHIDEE	PISCES	No	γ	Krinner et al. (2005)
	MIROC-ESM	MATSIRO and SEIB-DGVM	COCO	No	β	Watanabe et al. (2011)
	MPI-ESM-LR	JSBACH	HAMOCC5	No	β	Giorgetta et al. (2013)
	NorESM1-ME	CLM4	HAMOCC5	Yes	$\gamma + \beta$	Tjiputra et al. (2013)
CMIP6	ACCESS-ESM1-5	CABLE2.4 with CASA-CNP/	WOMBAT	Yes (p-cycle)	$\gamma + \beta$	Law et al. (2017) and Ziehn et al. (2017)
	CanESM5	CLASS-CTEM	CMOC	No	$\gamma + \beta$	Swart et al. (2019)
	CESM2	CLM5	MARBL	Yes	γ	—
	CNRM-ESM2-1	ISBA-CTRIP	PISCESv2-gas	No	$\gamma + \beta$	Decharme et al. (2019)
	GFDL-ESM4	LM4p1	COBALTv2	No	$\gamma + \beta$	Dunne et al. (2019)
	MPI-ESM1-2-LR	JSBACH3.2	MPIOM1.6 + HAMOCC6	Yes	β	Mauritsen et al. (2019)
	MRI-ESM2-0	HAL	MRI.COMv4	No	β	Yukimoto et al. (2019)
	NorESM2-LM	CLM5	HAMOCC5.1	Yes	$\gamma + \beta$	Seland et al. (2020)
	UKESM1-0-LL	JULES-ES1.0	NEMO + MEDUSA-2	Yes	$\gamma + \beta$	Sellar et al. (2019)

robustness of the existing emergent constraints and to increase the statistical significance that was rather limited in the original studies due to the small number of available ESMs. It is important to note that CMIP6 and CMIP5 models are not entirely independent from another. The latest generation of models are developed based on previous versions, which have (at least partly) participated in CMIP5. However, the verification of both previously derived emergent relationships from the CMIP5 models with the new generation of ESMs provides still useful evidence to confirm the existence of the emergent constraints.

In order to directly compare to W14 and W16, we use the same methods, but an extended historical time period up to 2014 for the larger ensemble of models in order to quantify both carbon cycle feedback parameters. In this study, we use model output from seven CMIP5 models and nine CMIP6 models (see Table 1). Not all models are participating in both analysis sections, due to data availability, which is explicitly indicated in Table 1. Each model performed three different simulation experiments which are listed in Table 2. We downloaded all models from the Earth System Grid Federation (ESGF) archive, which provided all necessary data (see Table S1 in Supporting Information S1) to diagnose the required quantities.

Table 2
Overview of the Model Simulation Experiments Used in This Study for CMIP5 and CMIP6

	Experiment	Coupling of carbon cycle	Available period	Forcing
CMIP5	esmHistorical	Fully coupled	1850–2005	Greenhouse gases, anthropogenic and volcanic climate forcing, land use change, solar forcing, and aerosols
	Extended by esmrcp85		2006–2099	
	1pctCO2	Fully coupled	0–140	1%/yr CO_2 increase
	esmFixClim1	Uncoupled	0–140	1%/yr CO_2 increase
CMIP6	esm-hist	Fully coupled	1850–2014	Greenhouse gases, anthropogenic and volcanic climate forcing, land use change, solar forcing, and aerosols
	1pctCO2	Fully coupled	0–140	1%/yr CO_2 increase
	1pctCO2-bgc	Uncoupled	0–140	1%/yr CO_2 increase

In the CMIP5 ensemble only two models (CESM1 and NorESM2-LM) included an interactive nitrogen cycle, but in the CMIP6 ensemble six models include this feature (see Table 1). One model, ACCESS-ESM1-5, additionally includes a phosphorus cycle. Models with interactive nutrient cycles are expected to have weaker CO_2 fertilization as they explicitly account for nutrient limitations on plant photosynthesis under higher CO_2 concentration (Thornton et al., 2007; Zaehle et al., 2010). However, models including an interactive nitrogen cycle are also expected to show a less negative impact of warming on land carbon storage, as warming of the soil increases nitrogen availability, as well as accelerating the decomposition of organic matter.

We use emission-driven historical simulations (*esm-hist*; Eyring et al., 2016a) for the period of 1860–2014, where atmospheric greenhouse gas concentrations are simulated rather than prescribed. For the CMIP5 models, we extend the *esmHistorical* simulation (Taylor et al., 2012) that ends in 2005 with the first 10 years of the *esmrcp85* future projections (see Table 2). The choice of climate scenario is not significant for such a short extension period. Additionally, for diagnosing the carbon cycle feedbacks, we use idealized simulations, where the increase of CO_2 concentration in the atmosphere is prescribed by 1% per year until quadrupling (*1pctCO2*; Eyring et al., 2016a). To analyze the relative importance of CO_2 fertilization and climate change on future carbon uptake, we compare the historical simulation with a biogeochemically coupled simulation which excludes climate change effects on the carbon cycle and has a prescribed atmospheric CO_2 increase of 1% per year until $4 \times CO_2$ (*1%BGC*; Jones et al., 2016), starting from a preindustrial value for 1850 of ∼285 ppmv.

2.2. Observations

For the sensitivity of global land carbon fluxes to tropical temperatures, which is used to constrain the carbon-climate feedback, we use the latest data from the Global Carbon Project (GCP; Friedlingstein et al., 2020). GCP provides a CO_2 budget including a report on the fossil fuel and the land use change emission data, the observed atmospheric CO_2 growth rate, an estimate of the ocean carbon uptake from nine ocean biogeochemical models constrained by observed oceanic uptake data, and an estimate of land carbon uptake from 17 Dynamical Global Vegetation Models (DGVM), constrained by observed carbon flux data. For our study, we used the residual of atmospheric carbon and ocean carbon sink for the land carbon sink, to avoid any circularity with using a DGVM-derived flux to evaluate the ESMs. The GCP data set covers the period from 1959 to the present, and is updated each year. The most recent changes are listed in the annually updated publications of the GCP project (e.g., Friedlingstein et al., 2020).

The IAV in the tropical near-surface temperature (30°S–30°N) is calculated using annual mean temperatures from the NOAA-National Climate Data Center (NCDC, http://www.esrl.noaa.gov/psd/data/gridded/data.noaamerged-temp.html). This data set covers the period from 1880 to present at a monthly resolution.

The observed range in the sensitivity of the CO_2 seasonal cycle amplitude to rising atmospheric CO_2 levels is diagnosed from in situ measurements at Pt. Barrow in Alaska. This data is provided by the National Oceanic and Atmospheric Administration (NOAA)/Earth System Research Laboratory (ESRL, http://www.esrl.noaa.gov/gmd/ccgg/trends) and covers a period from 1979 to present. The measuring site is a high-latitude station much less affected by midlatitude agriculture.

2.3. Emergent Constraints on Carbon Cycle Feedbacks

The carbon cycle feedback parameters are generally estimated following Friedlingstein et al. (2006), with additional assumptions made by W14 and W16 for the CMIP5 models and errors given as standard deviations. Here, we adopt these methods, which are summarized below.

The carbon cycle-climate feedback parameter γ_{LT} is derived from the difference between the land carbon storage of the coupled (1%COU) and uncoupled (1%BGC) simulations, and the temperature change in the coupled simulation, following W14. The subscript "LT" denotes the long-term response of the carbon cycle to climate change. Similar to W14, the changes in these variables are computed for the tropical land (30°N–30°S) as the absolute change between year 30 and year 110 after the start of the simulation. γ_{LT} is constrained by γ_{IAV}, which is the sensitivity of the Net Biome Productivity (NBP) to interannual changes in tropical near-surface temperature. In contrast to W14, we use NBP only to diagnose γ_{IAV}, rather than a combination of land and ocean carbon

fluxes. The short-term response of the carbon cycle to changes in near-surface temperature, γ_{IAV}, is derived from emission-driven historical simulations.

Similar to W16, the carbon cycle-CO_2 feedback is diagnosed from the fractional change over time of the GPP between 1860 and 1930 from the uncoupled (1%BGC) simulations only. For each model, the CO_2 fertilization factor is diagnosed individually for the northern Hemisphere high latitudes (60°N–90°N) for a doubling of atmospheric CO_2 concentration from its preindustrial value of 285 ppmv. Not all models provide output from year zero; therefore, the fractional change was calculated from 5-year means centered on year 10 and year 70. To account for the missing first 10% of the CO_2 increase the fraction was divided by a factor of 0.9. W16 found that the fractional change of GPP can be constrained by the sensitivity of the CO_2 seasonal cycle amplitude to increasing atmospheric CO_2 concentrations. For this, first the amplitude of the seasonal cycle is derived as the difference between the maximum and minimum monthly mean atmospheric CO_2 concentrations for each year. Second, we diagnose the slope of the linear regression of amplitude versus CO_2 concentration for those, over the full length of the records available from the observations and the historical model simulations (1860–2014) for the CMIP5 and CMIP6 models, in order to estimate the effect of increasing atmospheric CO_2 concentrations on the seasonal CO_2 cycle.

For both carbon cycle feedbacks, we use emergent constraints to derive observational constraints on the corresponding feedback parameters. Emergent constraints use an intermodel relationship (the so-called "emergent relationship") between a target quantity (here: carbon cycle feedback parameters) and an observable diagnostic from the past or present-day climate to derive a constraint for the target variable. To avoid spurious correlations, it is important that these relationships are based on robust physical mechanisms (e.g., Caldwell et al., 2014). Ultimately, emergent constraints provide a probabilistic estimate of the target variable in the form of a probability density function (PDF) based on the emergent relationships and observations of the Earth system. Details on the exact derivation of this PDF can be found in various other studies (e.g., Chai et al., 2021; Cox et al., 2018; Schlund et al., 2020).

2.4. ESMValTool

In order to ensure that the emergent constraints can be repeated on new model simulations, we implemented all routines into the new version of the Earth System Model Evaluation Tool (ESMValTool) version 2.3 (Eyring et al., 2020; Lauer et al., 2020; Righi et al., 2020; Weigel et al., 2021). The ESMValTool is an open-source community diagnostics and performance metrics tool for the evaluation of ESMs (https://www.esmvaltool.org/) that also ensures provenance. A specific ESMValTool recipe was written that can be used to reproduce the figures of this paper.

3. Results

As shown in Figure 1, the change in tropical land carbon storage shows a wide spread among the ensembles of CMIP5 and CMIP6 models. The spread in the full (CMIP5 and CMIP6) ensemble of models is of the order of 1,200 GtC for the coupled runs (1%COU, Figures 1a and 1b), with a minimum of 50 GtC (ACCESS-ESM1-5) to a maximum of 1,250 GtC (CanESM5); and 1,250 GtC for the uncoupled runs (1%BGC, Figures 1c and 1d), from 200 GtC (ACCESS-ESM1-5) to 1,450 GtC (CanESM5)). It is interesting to note that the boundaries of the spread are dominated by CMIP6 models, where especially CanESM5 increases the spread by simulating a high NBP increase in the coupled and uncoupled simulations (Davies-Barnard et al., 2020), respectively. Therefore, Figure 1 underlines the need of further constraining carbon cycle feedbacks with observations in particular since in the new set of CMIP6 models the spread in the future projections of land carbon sink even increases compared to CMIP5.

3.1. Emergent Constraint on the Carbon-Climate Feedback

From the quantities shown in Figure 1, the climate-carbon cycle sensitivity γ_{LT} can be quantified in terms of carbon loss per unit temperature increase from the difference of coupled and uncoupled simulations. γ_{LT} values for each model are shown in Figure 2 and listed in Table 3. As found by previous studies (Arora & Boer, 2013; Arora et al., 2020; Cox et al., 2000; Friedlingstein, 2001; Friedlingstein et al., 2006; Sabrina Wenzel et al., 2014),
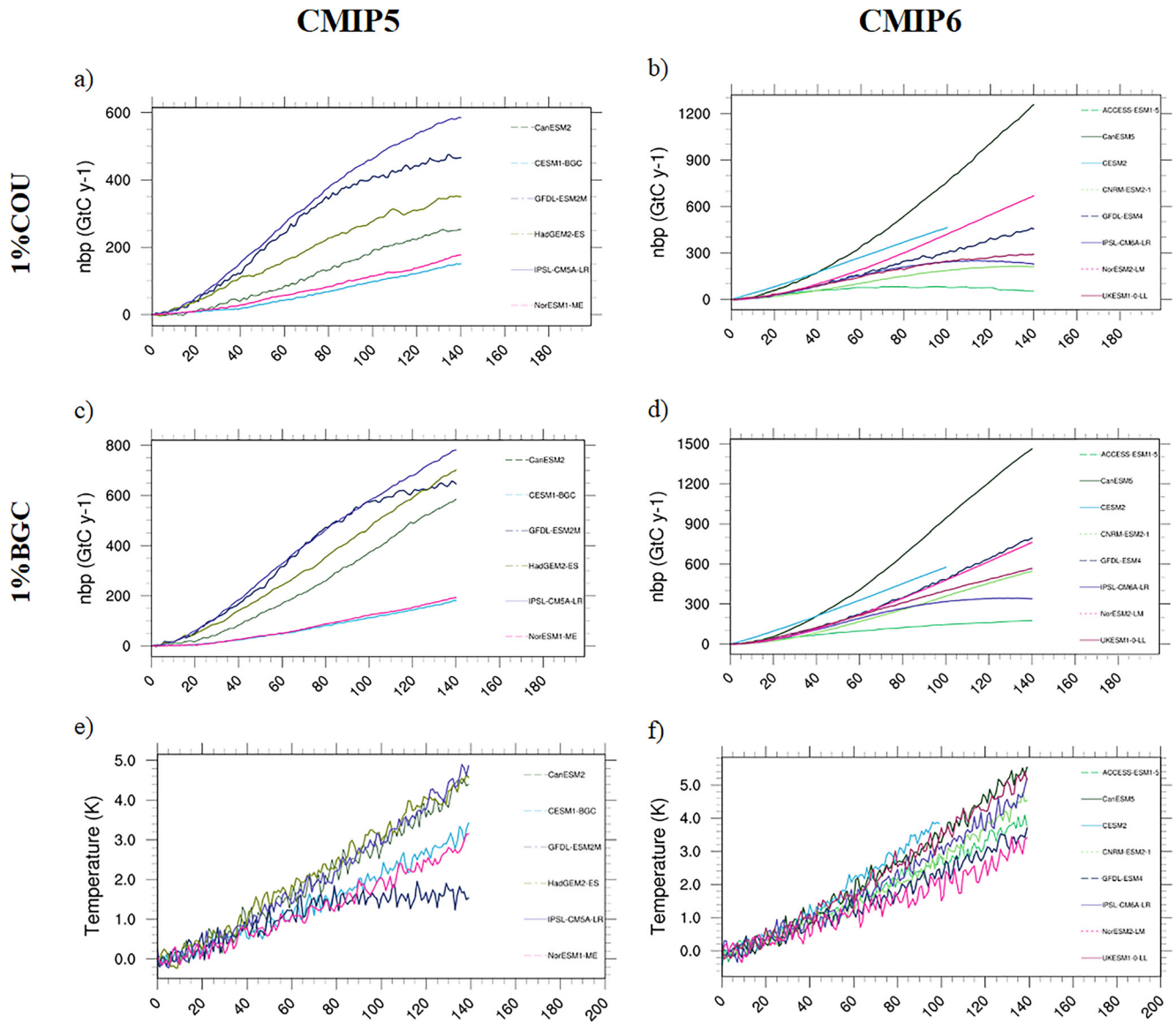
Figure 1. Tropical (30°N–30°S) quantities to quantify γ_{LT} from CMIP5 (left panels) and CMIP6 (right panels) models. Cumulated NBP from (a, b) coupled and (c, d) uncoupled simulations. (e, f) Averaged near-surface air temperature anomalies from coupled simulation.

γ_{LT} is negative for all models. However, there is a wide range of results in γ_{LT} (Figure 2a), from −7 GtC/K in CESM1-BGC to −135 GtC/K in GFDL-ESM2M (see Table 3). Interestingly, the maximum range is still given by same models from the CMIP5 ensemble as shown by W14, even though the CMIP6 models show a larger spread of changes in tropical land carbon storage. The CMIP6 ensemble estimates of γ_{LT} only range between −27 ± 4 GtC/K (CESM2) and −94 ± 6 GtC/K (GFDL-ESM4). Hence, the intermodel spread in the carbon-climate feedback parameter has been reduced from CMIP5 to CMIP6 models.

W14 found that models from the CMIP5 model ensemble including an interactive nitrogen cycle show less negative γ_{LT} values. This finding is also true for the CMIP6 models that include a nitrogen cycle and for one model (ACCESS-ESM1-5) that additionally includes a phosphorus cycle. Among these models, the lowest values are simulated by the UKESM1-0-LL model with −48 ± 4 GtC/K.

For consistency with the CO_2 observational data, γ_{IAV} is calculated for the period 1960–2014 from the historical simulations shown in Figure 2b. γ_{IAV} varies in the CMIP5 and CMIP6 model ensemble from close to zero
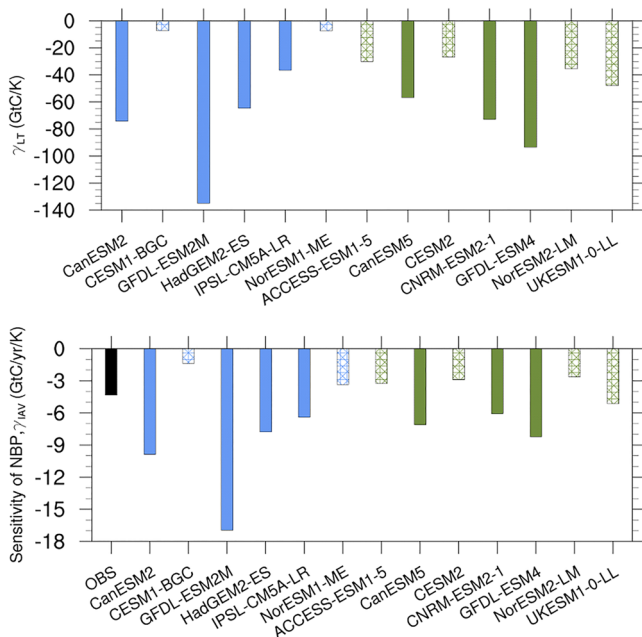
Figure 2. Sensitivities for the individual CMIP5 (blue) and CMIP6 (green) models showing (a) the long-term sensitivity of tropical (30°N–30°S) NBP due to rising near-surface tropical temperature using 1% CO_2 BGC simulations (1880–1960) and (b) the short-term sensitivity of Net Biome Productivity (NBP) due to interannual changes in the near-surface temperatures using esm-hist simulations (1960–2014) and observations (black). Hashed bars indicate models including a N-cycle.

(nonsignificant) for CESM1-BGC to −17 GtC/yr/K for GFDL-ESM2M, with a multimodel average of −5.5 ± 1.9 GtC/yr/K (Figure 2b).

From the GCP land carbon fluxes versus the IAV of tropical (30°S–30°N) temperature from NCDC data, we derive an observed value for γ_{IAV} of −4.06 ± 0.67 GtC/yr/K. This is similar to W14 and well within the range of previous studies (Cox et al., 2013).

Comparing the values for γ_{LT} and γ_{IAV} (Figure 2), it is evident that the models that show a high (low) carbon cycle-climate feedback parameter γ_{LT}, also show a high (low) short-term sensitivity of land and ocean carbon fluxes to tropical warming γ_{IAV}, as found in W14 for CMIP5 models. Correlating both values and accounting for the observed γ_{IAV} reveals the emergent constraint shown in Figure 3. As previously found by Cox et al. (2013) and W14, it shows a clear linear relationship for the individual CMIP ensembles (CMIP5: $R^2 = 0.97$, CMIP6: $R^2 = 0.84$) as well as for the combined CMIP5 and CMIP6 ensembles ($R^2 = 0.86$).

Including the CMIP6 models within the ensemble of models reduces the sharpness of the unconstrained model PDF. This is especially because the CMIP6 ensemble tends to generally estimate lower values for γ_{LT} than the CMIP5 models have (Table 3). Additionally, they also have a weaker linear relation between the short and long-term response of the carbon cycle to climate warming than the CMIP5 ensemble.

Generally, CMIP6 models cluster more around the observational range, in itself slightly narrowing the range of γ_{LT} to −52 ± 35 GtC/K (Figure 3b) in the CMIP6 ensemble compared to −49 ± 40 GtC/K for the CMIP5 ensemble alone (W14). We can also confirm the findings of W14 that models including interactive nutrient cycles still fit on this linear relationship. This underlines

Table 3
Summary of the Derived Sensitivities γ_{LT} and γ_{IAV} for Each Model, the Observations Used to Constrain the Carbon-Climate Feedback (See W14), and for the Multimodel Means of CMIP5 and CMIP6 and Combined

| Ensemble	Model	γ_{LT} (GtC/K)	γ_{IAV} (GtC/yr/K)
CMIP5	CanESM2	−74.21 ± 7.2	−9.87 ± 0.86
	CESM1-BGC	−7.27 ± 7.0	−1.37 ± 1.16
	GFDL-ESM2M	−134.95 ± 9.3	−16.96 ± 2.06
	HadGEM-ES	−64.60 ± 6.4	−7.77 ± 0.72
	IPSL-CM5A-R	−36.61 ± 4.7	−6.72 ± 1.14
	NorESM1-ME	−7.47 ± 4.3	−3.34 ± 1.14
CMIP6	ACCESS-ESM1-5	−30.01 ± 5.7	−3.23 ± 0.57
	CanESM5	−56.38 ± 4.4	−7.10 ± 0.94
	CESM2	−26.86 ± 3.6	−2.89 ± 0.39
	CNRM-ESM2-1	−72.87 ± 5.7	−6.07 ± 0.99
	GFDL-ESM4	−93.55 ± 6.1	−8.22 ± 0.87
	NorESM2-LM	−35.44 ± 3.0	−2.64 ± 0.39
	UKESM1-0-LL	−47.93 ± 3.6	−5.13 ± 0.62
	OBS	–	−4.30 ± 0.67
	CMIP5 model mean	−54 ± 40	−7.67 ± 1.17
	CMIP6 model mean	−51 ± 35	−5.04 ± 0.68
	CMIP5 + CMIP6 model mean	−52 ± 39	−6.25 ± 0.91
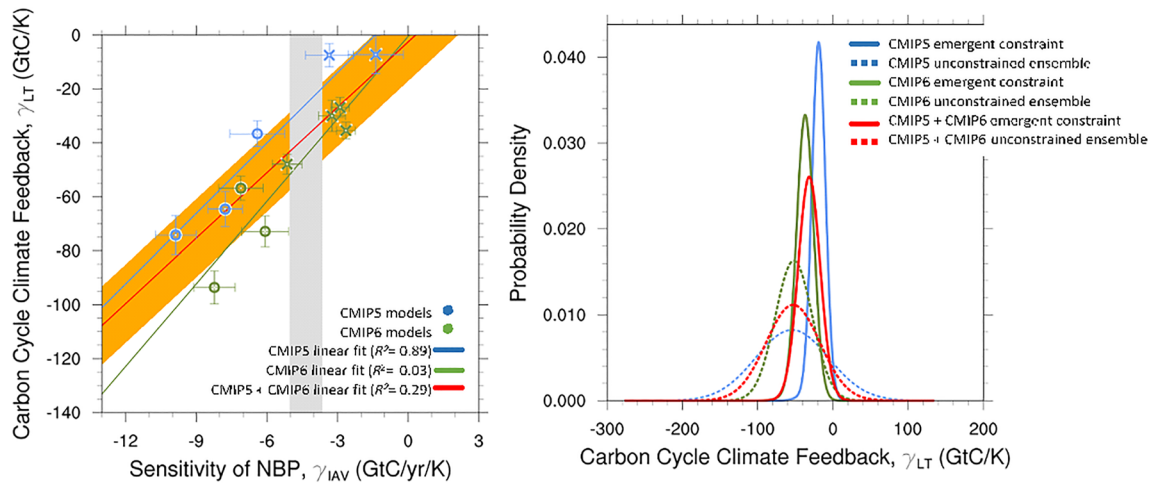
Figure 3. Emergent constraint on the carbon cycle-climate feedback. (a) Long-term sensitivity of tropical land carbon storage to climate warming (γ_{LT}) versus the short-term sensitivity of atmospheric CO_2 to interannual temperature variability (γ_{IAV}) for the CMIP5 (blue) and CMIP6 (green) models. The red line shows the best-fit line across all models, whereas the blue and green line correspond to the CMIP5 and CMIP6 ensemble. The orange shaded area represents the standard prediction error for the linear regression including all models, and the gray shaded area shows the range of the observed γ_{IAV} according to Figure 2 (mean ± one standard deviation). Crosses denote models including a nitrogen cycle. (b) Probability density function (PDF) for γ_{LT}. The solid lines were derived after applying the interannual variability (IAV) constraint model ensembles while the dashed lines are the corresponding prior PDFs, derived purely from the models, before applying the IAV constraint.

that the inclusion of a nitrogen cycle as well as a phosphorus cycle does not seem to change the relationship between the short and the long-term responses of tropical land carbon to climate.

By constraining the individual CMIP ensembles and the whole model ensemble with the observed γ_{IAV}, conditional PDFs can be calculated (Cox et al., 2013). The PDF for the combined CMIP ensemble reveals a constraint value for γ_{LT} of -37 ± 14 GtC/K which is well within the uncertainty range of W14's diagnosed value of -44 ± 14 GtC/K. The PDF for the observationally constrained value of γ_{LT} shows a sharper peak than the PDF derived from the raw model ensembles, implying that this emergent constraint has successfully reduced the uncertainty in γ_{LT}.

3.2. Emergent Constraint on the Carbon-Concentration Feedback

The fertilization effect of increasing CO_2 concentrations on plant photosynthesis has been quantified by W16 as the fractional change in GPP due to doubling of the atmospheric CO_2 concentrations. This study repeats that analysis but focuses on the high-latitude site (Pt. Barrow, Alaska) only. Therefore, Figures 4a and 4b show the high-latitude (60°–90°N) annual mean GPP versus the annual global mean atmospheric CO_2 concentrations for the 1%BGC runs of the CMIP5 and CMIP6 models. All models show a positive response of GPP to increasing atmospheric CO_2 concentrations (Table 4 and Figure 5a), with the smallest response given by CanESM5 with about 8% increase and the largest increase given by CNRM-ESM2-1 with about 65%.

For CMIP5, W16 found that the magnitude of the high-latitude CO_2 fertilization effect is well-correlated with the rate at which the amplitude of the CO_2 seasonal cycle increases with annual mean CO_2 at Pt. Barrow from 1860 to 2014. Following W16, Figures 4c and 4d show the CO_2 seasonal amplitude versus the annual mean atmospheric CO_2 concentrations at Pt. Barrow for the historical simulations of the CMIP5 and CMIP6 models. In these figures, the sensitivity of the CO_2 seasonal cycle amplitude to CO_2 can be diagnosed by the slope of a linear regression between the two variables. These slopes are plotted in Figure 5b, which shows a positive linear trend for all CMIP5 and CMIP6 models over the period 1860–2014 (ranging from 0.015 to 0.074 ppmv/ppmv) and for observations from the ESRL over the period 1960–2014 (0.055 ± 0.007 ppmv/ppmv). The CMIP5 models show a higher variation in the sensitivity of the CO_2 amplitude to atmospheric CO_2 increase from 0.015 to 0.074 ppmv/ppmv and tend to underestimate the observed value. On the contrary, the CMIP6 models only span a range of 0.041–0.073 ppmv/ppmv, which is more consistent with the observed range measured by ESRL.

As already shown by W16, for the CMIP5 models, the high-latitude (60°–90°N) GPP response to increasing CO_2 in the 1%BGC run (y-axis) is well-correlated with the change in the CO_2 seasonal cycle amplitude at Pt. Barrow
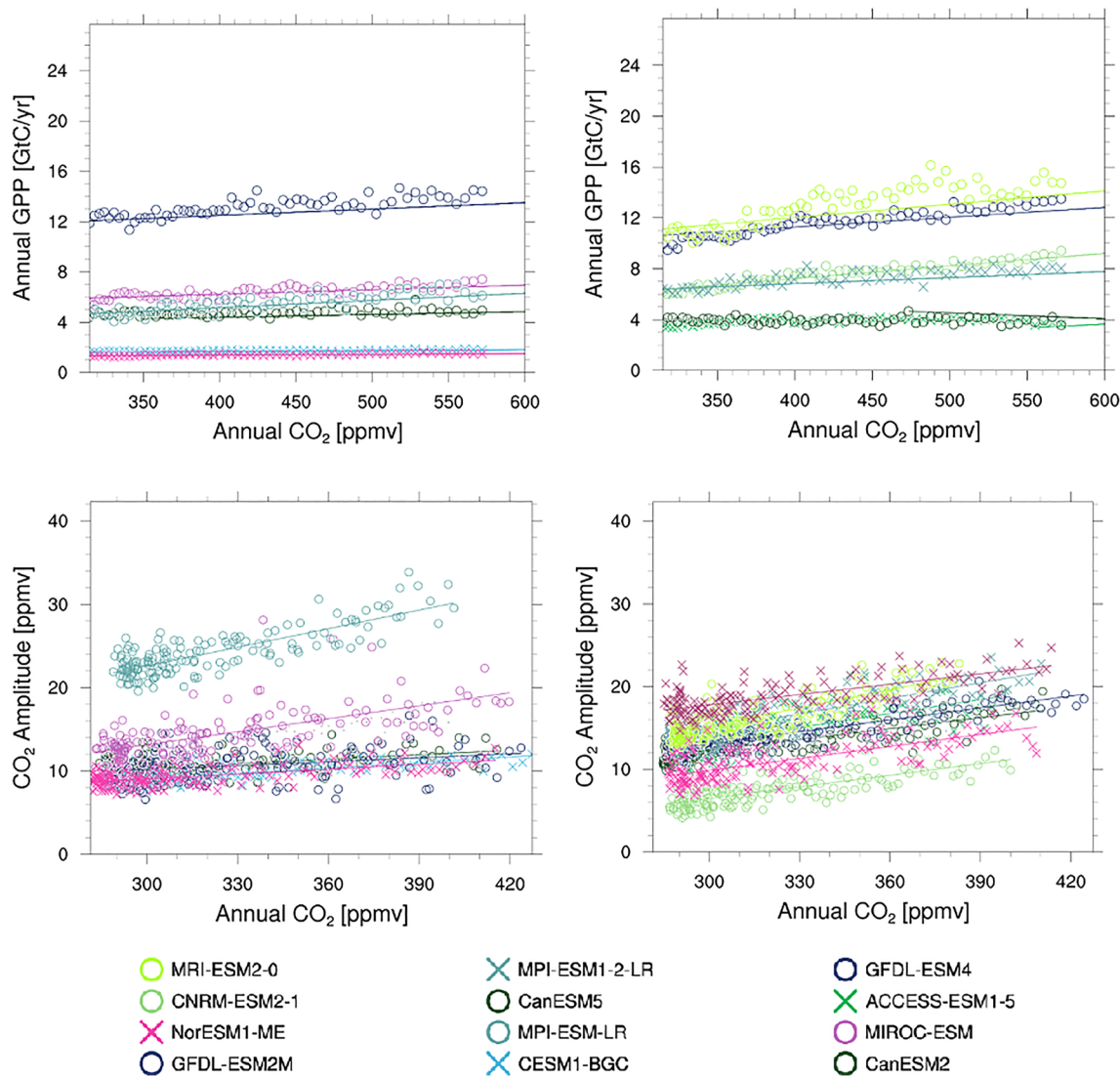
Figure 4. Upper panels: Annual global mean CO_2 change versus the annual mean high-latitude Gross Primary Productivity (GPP) in CMIP5 (left) and CMIP6 (right) models. Lower panels: Annual mean atmospheric CO_2 concentration versus the amplitudes of the CO_2 seasonal cycle at Pt. Barrow from historical simulations (1860–2014) and observations (black).

(*x*-axis; see blue markers in Figure 6). However, in the uncoupled 1%BGC simulations (blue circles in Figure 6a), the annual mean high-latitude GPP shows a weaker response to increasing CO_2 than in the historical simulations (blue crosses in Figure 6a). A similar positive correlation can be found for the CMIP6 models (green markers in Figure 6). Some of these CMIP6 models show higher differences in the GPP response to CO_2 between the (fully coupled) historical and 1%BGC runs, which implies that additional climate change effects (e.g., changes in surface temperature, changes in precipitation) contribute to the increase in GPP apart from the CO_2 fertilization effect alone. Variations in GPP response to climate or CO_2 across models are partly due the fact that only a subset of the models includes a nitrogen cycle, but also to the representation of underlying processes relevant to GPP such as carbon allocation, and interaction with the hydrological cycle (e.g., Lian et al., 2018). However, the assumption W16 made, that "the change in CO_2 amplitude remains strongly correlated with the strength of the CO_2 fertilization across the model ensemble" is still valid. In addition, Schlund et al. (2020) show that the emergent relationship proposed by W16 also holds for fully coupled CMIP5 Representative Concentration Pathway (RCP) 8.5 simulations, which further corroborates W16's assumption.

Correlating the CO_2 fertilization effect with the observable short-term sensitivity of the atmospheric CO_2 seasonal cycle amplitude to CO_2 increase follows the relationship as presented in Figure 7a. The linear best-fit lines for

Table 4
Summary of the Changes in High-Latitude GPP (60°–90°N) at a Doubling of Atmospheric CO_2 Concentrations and the Amplitude of the CO_2 Seasonal Cycle at Pt

Ensemble	Model	GPP(2 × CO2)/ GPP(1 × CO2)	Offset to initial amplitude, $a0$ (ppmv)	CO_2 sensitivity of amplitude, a (ppmv/ppmv)
CMIP5	CanESM2	1.16 ± 0.04	4.84 ± 0.88	0.018 ± 0.002
	CESM1-BGC	1.22 ± 0.04	2.30 ± 0.49	0.022 ± 0.001
	GFDL-ESM2M	1.25 ± 0.05	5.40 ± 1.37	0.015 ± 0.004
	MIROC-ESM	1.41 ± 0.06	−2.45 ± 1.60	0.052 ± 0.004
	MPI-ESM-LR	1.47 ± 0.12	0.28 ± 1.38	0.074 ± 0.004
	NorESM1-ME	1.25 ± 0.05	3.17 ± 0.68	0.019 ± 0.002
CMIP6	ACCESS-ESM1-5	1.19 ± 0.04	−6.41 ± 1.96	0.055 ± 0.005
	CanESM5	1.08 ± 0.07	−1.00 ± 0.93	0.044 ± 0.002
	CNRM-ESM2-1	1.65 ± 0.04	−8.61 ± 1.21	0.047 ± 0.003
	GFDL-ESM4	1.49 ± 0.06	−2.43 ± 0.93	0.048 ± 0.002
	MPI-ESM1-2-LR	1.41 ± 0.06	−4.47 ± 1.44	0.062 ± 0.003
	MRI-ESM2-0	1.49 ± 0.07	−6.10 ± 1.60	0.073 ± 0.004
	NorESM2-LM	1.32 ± 0.11	−5.01 ± 1.59	0.048 ± 0.004
	UKESM1-0-LL	1.39 ± 0.045	−5.68 ± 1.34	0.041 ± 0.003
	OBS	–	−6.95 ± 3.84	0.055 ± 0.007
	CMIP5 mean	1.29 ± 0.06	–	0.036 ± 0.002
	CMIP6 mean	1.37 ± 0.11	–	0.052 ± 0.003
	CMIP5 + CMIP6 mean	1.34 ± 0.09	–	0.046 ± 0.003

Note. Barrow, Alaska used to constrain the carbon-concentration feedback (see W16) for the individual models as well as for the multimodel means of CMIP5 and CMIP6 and combined.

the CMIP5 and CMIP6 ensembles are similar; however, the CMIP6 models cluster around the observational range on the *x*-axis but not around the *y*-axis. As a consequence, the emergent relationship in CMIP6 ($R^2 = 0.03$) is much weaker than in CMIP5 ($R^2 = 0.89$). When combining the results of both CMIP ensembles, the linear relation is not as strong ($R^2 = 0.29$) and tight (in terms of the standard prediction error of the linear regression; see orange shaded area in Figure 7a) as estimated by W16 for the CMIP5 ensemble alone. We estimate a multimodel mean CO_2 fertilization effect of 34 ± 15% for all participating CMIP models. The multimodel range is much wider for CMIP6 with some models showing very high (CNRM-ESM2-1) and very low (CanESM5) GPP responses (see also Table 4). Nevertheless, CMIP6 models that do include an interactive nitrogen cycle show a smaller intermodel spread in the CO_2 fertilization than models that do not include this. Similar to the previous section, we calculate the PDFs for the unconstrained and constrained (using the CO_2 observations of ESRL at Pt. Barrow) model ensembles, both for the CMIP5, CMIP6, and combined ensemble (see Figure 7b). The combined constrained ensemble gives a CO_2 fertilization effect of 39 ± 13%, which is consistent with the constraint reported by W16 (37 ± 9%). As expected by the emergent relationships in Figure 7a, the constrained PDF for the CMIP5 ensemble is much tighter than its CMIP6 counterpart, which indicates that the emergent relationship is weaker when applied to the CMIP6 models. Therefore, a further reduction of the uncertainty with the emergent constraint of W16 cannot be achieved by including the CMIP6 ensemble.

Figure S1 in Supporting Information S1 shows a summary of both constrained carbon cycle feedbacks evaluated on the CMIP5 and CMIP6 models. For the carbon cycle-climate feedback (*y*-axis), the CMIP6 models (green) show a slightly better agreement with the observational constraint (horizontal dashed lines) than the CMIP5 models (blue). For the carbon cycle-concentration feedback (*x*-axis), CMIP5 models consistently underestimate the constrained feedback strength (vertical dashed lines), while CMIP6 models overestimate and underestimate it. Notably, two CMIP6 models agree with both observational constraints (gray shaded area); both models use an interactive nitrogen cycle. Moreover, models that use an interactive nitrogen cycle (crosses) tend to agree better
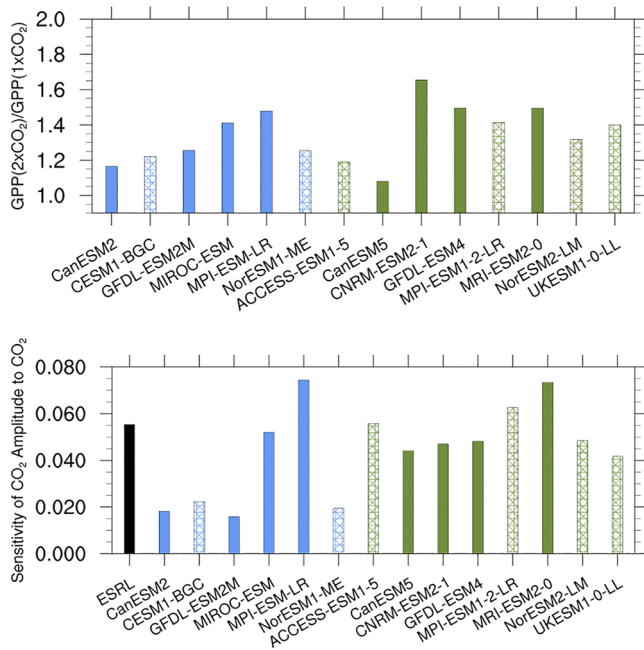
Figure 5. (a) Bar chart showing the relative change in high-latitude Gross Primary Productivity (GPP) at a doubling of CO_2 in the 1%BGC simulations (1860–1920) in CMIP5 (blue) and CMIP6 (green) models. (d) Bar chart showing the corresponding gradient of the linear regressions from Figure 4b at Pt. Barrow.

with the observational constraints than models without an interactive nitrogen cycle (circles). Note that only models are shown that provide the necessary data to diagnose both carbon cycle feedbacks.

4. Summary and Conclusions

In this study, two previously published observationally based constraints on carbon cycle feedbacks are evaluated on ESMs participating in CMIP6. In this new phase of model intercomparison, the size of the land carbon sink in future projections still varies widely across the ensemble (Arora et al., 2020) and remains a key uncertainty. To test the robustness of both emergent constraints, nine models from CMIP6 are added to the already existing ensemble of seven CMIP5 models, increasing the total number of participating ESMs to 15. The CMIP6 models can be used to perform out-of-sample tests of the emergent constraints since these new ESMs have not been used to derive the emergent relationships in the original publications.

In the first part of this study, the tropical land carbon cycle-climate feedback parameter γ_{LT} is constrained using the short-term sensitivity of the atmospheric CO_2 growth rate to IAV in the near-surface tropical temperature γ_{IAV}. This is a continuation of past studies that analyzed this emergent constrained for the CMIP5 ensemble (W14) and the C4MIP ensemble (Cox et al., 2013). Similar to these previous analyses, we find a strong linear relationship between γ_{LT} and γ_{IAV} for the CMIP6 models, indicating that the emergent relationship still holds in the CMIP6 ensemble. The linear fits for the CMIP5 and CMIP6 models are very similar, which further corroborates the robustness of this emergent constraint. Additionally, in both ensembles, ESMs with an interactive nitrogen cycle exhibit higher (i.e., less negative) values for γ_{LT}

and γ_{IAV}. Using the combined ensemble of CMIP5 and CMIP6 models, we find an observational constraint of -37 ± 14 GtC/K for γ_{LT}. This is fully consistent with the uncertainty range given by W14 of -44 ± 14 GtC/K for the CMIP5 models alone. In contrast to that, the multimodel mean of the combined ensemble is -52 ± 35 GtC/K; therefore, the uncertainty range can be reduced by 60% using the emergent constraint. Moreover, we find that the CMIP6 models exhibit a smaller intermodel range in γ_{IAV} (x-axis of the emergent constraint) than the CMIP5 models which is also more consistent to the observations. This suggests that the new CMIP6 models include a
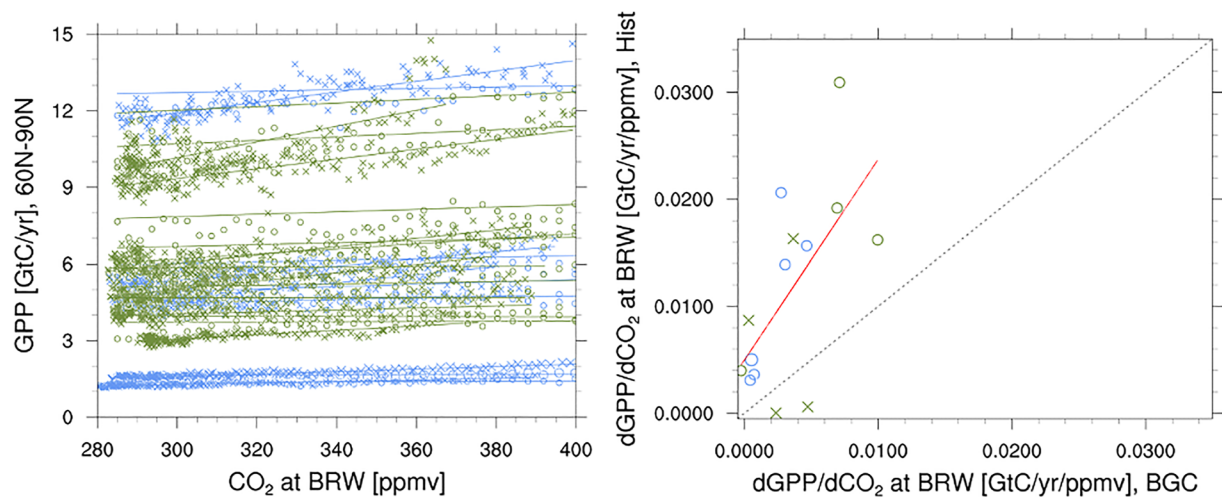

Figure 6. (a) The correlation between the change in high-latitude Gross Primary Productivity (GPP) and the annual CO_2 at Pt. Barrow (BRW) for both, the historical (asterisks) and the 1%BGC (circles) CMIP5 (blue) CMIP6 (green) model simulations. The markers show the values for the individual years and lines show the linear best-fit for each CMIP5 (blue) and CMIP6 (green) model. (b) The comparison of the gradients in (a) for each model. The red solid line shows the best-fit straightline and the black dashed line indicates a 1:1 relationship. Crosses denote models including a nitrogen cycle.
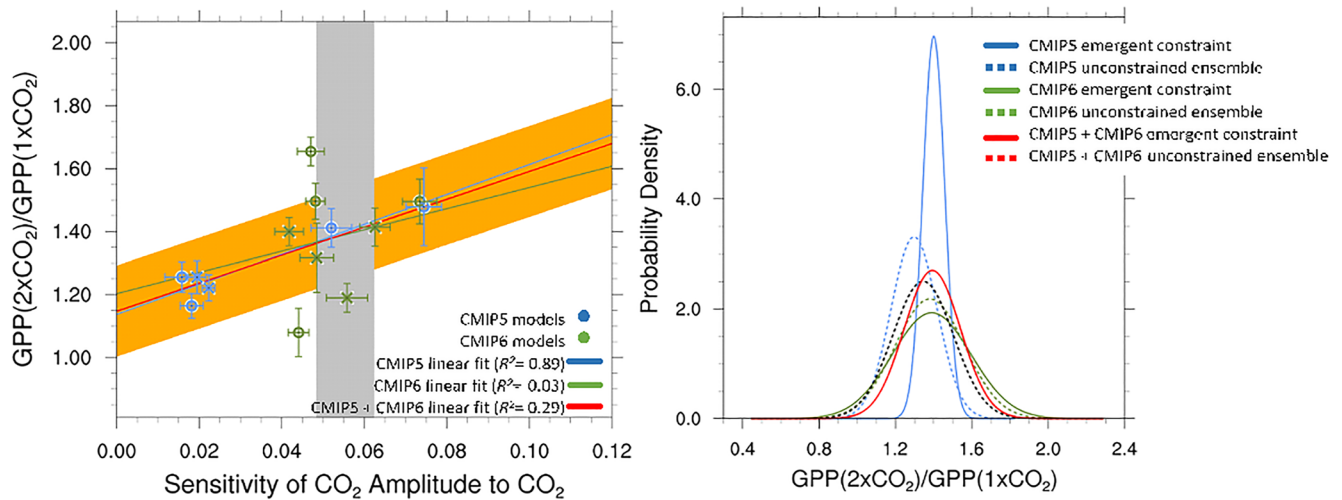
Figure 7. Emergent constraints on the relative increase of large-scale Gross Primary Productivity (GPP) for a doubling of CO_2. (a) Correlations between the sensitivity of the CO_2 amplitude to annual mean CO_2 increases at Pt. Barrow (x-axis) and the high-latitude (60°–90°N) CO_2 fertilization on GPP at $2 \times CO_2$) for the CMIP5 (blue) and CMIP6 (green) models. The red line shows the best-fit line across all models, whereas the blue and green line correspond to the CMIP5 and CMIP6 ensemble, respectively. The orange shaded area represents the standard prediction error for the linear regression including all models, and the gray shaded area shows the range of the observed CO_2 amplitude to annual mean CO_2 increases according to Figure 5 (mean ± one standard deviation). Circles and crosses denote models without and with a nitrogen cycle, respectively. (b) Probability density function (PDF) for the unconstrained CO_2 fertilization of GPP (dashed) and the conditional PDF arising from the emergent constraints (solid) for high-latitude GPP for CMIP5, CMIP6, and combined.

better representation of the sensitivity of the atmospheric CO_2 growth rate to short-term changes in the tropical temperature than the corresponding CMIP5 models.

The second part of the study focuses on an emergent constraint on the high-latitude carbon cycle-concentration feedback. Similar to the original publication (W16), we use the high-latitude (60°–90°N) CO_2 fertilization effect (diagnosed as the fractional GPP change at the time of CO_2 doubling in a 1%BGC run) as target variable and the sensitivity of the CO_2 seasonal cycle amplitude to increasing atmospheric CO_2 concentrations as an observational constraint. We find very similar emergent relationships (in terms of the linear fit) for the CMIP5 and CMIP6 ensembles; however, the correlation between the target variable and the observable is much weaker for the CMIP6 models. The reason for this is a clustering of the CMIP6 models around the observations on the x-axis without an accompanying reduction of the spread in the target variable on the y-axis. This suggests that the CMIP6 models exhibit an improved representation of the historical CO_2 seasonal cycle amplitude relative to the CMIP5 models; however, there is still a substantial spread in future CO_2 fertilization which even increased in CMIP6. Thus, the emergent constraint of W16 has reduced skill for the CMIP6 ensemble. This is further underpinned by the PDFs and uncertainty ranges that can be derived for this emergent constraint: For the combined model ensemble of CMIP5 and CMIP6 models, the observational constraint for the fractional GPP change at the time of CO_2 doubling is 39 ± 13%, which is consistent with the findings of W16 of 37 ± 9% for the CMIP5 models, but shows a considerably larger uncertainty range. Moreover, we find that CMIP6 models with an interactive nitrogen representation generally exhibit a smaller intermodel range in the CO_2 fertilization, which might be related to nutrient limitations of the terrestrial biosphere.

The weakening of the emergent relationships when moving from the CMIP5 to CMIP6 ensemble is not new: As shown by Schlund et al. (2020), multiple emergent constraint on the effective climate sensitivity derived for the CMIP3 or CMIP5 ensembles do not hold in CMIP6 anymore. Schlund et al. (2020b) hypothesize that the increased complexity of the CMIP6 models might be a possible reason for this loss of skill of the emergent constraints. A basic assumption of the emergent constraint approach is that a single observable process or physical aspect in the current climate dominates the uncertainty in the target variable. However, for the more complex ESMs of CMIP6 that include much more processes than their predecessor models, this assumption might not be valid anymore. Thus, a possible reason for the weakening of the W16 emergent relationship in CMIP6 is an improved simulation of the increasing CO_2 seasonal cycle amplitude that causes the models to cluster within observational uncertainty which is not accompanied by the necessary reduction in the spread of CO_2 fertilization. The latter might be explained by further processes that have been added to the land components of the more

complex CMIP6 models. Multivariate approaches such as those applied by Schlund et al. (2020a) should be further examined to help constraining uncertainties in climate projections.

Data Availability Statement

The corresponding recipe that can be used to reproduce the figures of this paper will be included in the ESMVal-Tool (Eyring et al., 2020; Lauer et al., 2020; Righi et al., 2020; Weigel et al., 2021) as soon as the paper is published. The new extensions described in this paper are available since ESMValTool v2.6.0. ESMValTool v2 is released under the Apache License, VERSION 2.0. The latest release of ESMValTool v2 is publicly available on Zenodo at https://doi.org/10.5281/zenodo.3401363 (Andela et al., 2022a). The source code of the ESMVal-Core package, which is installed as a dependency of ESMValTool v2, is also publicly available on Zenodo at https://doi.org/10.5281/zenodo.3387139 (Andela et al., 2022b). ESMValTool and ESMValCore are developed on the GitHub repositories available at https://github.com/ESMValGroup (last access: 1 August 2022). For further details, we refer to the ESMValTool documentation available at https://docs.esmvaltool.org/ (last access: 1 August 2022) and the ESMValTool website (https://www.esmvaltool.org/, last access: 1 August 2022).

References

Andela, B., Broetz, B., de Mora, L., Drost, N., Eyring, V., Koldunov, N., et al. (2022a). *ESMValTool*. https://doi.org/10.5281/zenodo.6900341

Andela, B., Broetz, B., de Mora, L., Drost, N., Eyring, V., Koldunov, N., et al. (2022b). *ESMValCore*. https://doi.org/10.5281/zenodo.6838798

Arora, V. K., Boer, G. J., Friedlingstein, P., Eby, M., Jones, C. D., Christian, J. R., et al. (2013a). Feedbacks in emission-driven and concentration-driven global carbon budgets. *Journal of Climate*, *26*(10), 3326–3341. https://doi.org/10.1175/jcli-d-12-00494.1

Arora, V. K., Boer, G. J., Friedlingstein, P., Eby, M., Jones, C. D., Christian, J. R., et al. (2013b). Carbon-concentration and carbon-climate feedbacks in CMIP5 Earth System Models. *Journal of Climate*, *26*(15), 5289–5314. https://doi.org/10.1175/jcli-d-12-00494.1

Arora, V. K., Katavouta, A., Williams, R. G., Jones, C. D., Brovkin, V., Friedlingstein, P., et al. (2020). Carbon-concentration and carbon-climate feedbacks in CMIP6 models, and their comparison to CMIP5 models. *Biogeosciences*, *17*, 4173–4222. https://doi.org/10.5194/bg-17-4173-2020

Arora, V. K., Scinocca, J. F., Boer, G. J., Christian, J. R., Denman, K. L., Flato, G. M., et al. (2011). Carbon emission limits required to satisfy future representative concentration pathways of greenhouse gases. *Geophysical Research Letters*, *38*, L05805. https://doi.org/10.1029/2010GL046270

Boer, G. J., & Arora, V. (2009). Temperature and concentration feedbacks in the carbon cycle. *Geophysical Research Letters*, *36*, L02704. https://doi.org/10.1029/2008GL036220

Caldwell, P. M., Bretherton, C. S., Zelinka, M. D., Klein, S. A., Santer, B. D., & Sanderson, B. M. (2014). Statistical significance of climate sensitivity predictors obtained by data mining. *Geophysical Research Letters*, *41*, 1803–1808. https://doi.org/10.1002/2014GL059205

Chai, Y., Martins, G., Nobre, C., von Randow, C., Chen, T., & Dolman, H. (2021). Constraining Amazonian land surface temperature sensitivity to precipitation and the probability of forest dieback. *npj Climate and Atmospheric Science*, *4*(1), 6. https://doi.org/10.1038/s41612-021-00162-1

Clark, D. B., Mercado, L. M., Sitch, S., Jones, C. D., Gedney, N., Best, M. J., et al. (2011). The Joint UK Land Environment Simulator (JULES), model description—Part 2: Carbon fluxes and vegetation dynamics. *Geoscientific Model Development*, *4*(3), 701–722. https://doi.org/10.5194/gmd-4-701-2011

Cox, P. M. (2001). Description of the "TRIFFID" Dynamic Global Vegetation Model. *Hadley Centre Technical Note*, *24*, 1–17. https://doi.org/10.1111/j.1747-1346.2001.tb00581.x

Cox, P. M., Betts, R. A., Jones, C. D., Spall, S. A., & Totterdell, I. J. (2000). Acceleration of global warming due to carbon-cycle feedbacks in a coupled climate model. *Nature*, *408*(6809), 184–187. https://doi.org/10.1038/35041539

Cox, P. M., Huntingford, C., & Williamson, M. S. (2018). Emergent constraint on equilibrium climate sensitivity from global temperature variability. *Nature*, *553*(7688), 319–322. https://doi.org/10.1038/nature25450

Cox, P. M., Pearson, D., Booth, B. B., Friedlingstein, P., Huntingford, C., Jones, C. D., & Luke, C. M. (2013). Sensitivity of tropical carbon to climate change constrained by carbon dioxide variability. *Nature*, *494*(7437), 341–344. https://doi.org/10.1038/nature11882

Davies-Barnard, T., Meyerholt, J., Zaehle, S., Friedlingstein, P., Brovkin, V., Fan, Y., et al. (2020). Nitrogen cycling in CMIP6 land surface models: Progress and limitations. *Biogeosciences*, *17*(20), 5129–5148. https://doi.org/10.5194/bg-17-5129-2020

Decharme, B., Delire, C., Minvielle, M., Colin, J., Vergnes, J. P., Alias, A., et al. (2019). Recent changes in the ISBA-CTRIP Land Surface System for use in the CNRM-CM6 Climate Model and in global off-line hydrological applications. *Journal of Advances in Modeling Earth Systems*, *11*, 1207–1252. https://doi.org/10.1029/2018ms001545

Dunne, J. P., Horowitz, L. W., Adcroft, A. J., Ginoux, P., Held, I. M., John, J. G., et al. (2019). The GFDL Earth System Model version 4.1 (GFDL-ESM4.1): Model description and simulation characteristics. *Journal of Advances in Modeling Earth Systems*, *12*, e2019MS002015. https://doi.org/10.1029/2019MS002015

Dunne, J. P., John, J. G., Adcroft, A. J., Griffies, S. M., Hallberg, R. W., Shevliakova, E., et al. (2012). GFDL's ESM2 Global Coupled Climate-Carbon Earth System Models. Part I: Physical formulation and baseline simulation characteristics. *Journal of Climate*, *25*(19), 6646–6665. https://doi.org/10.1175/jcli-d-11-00560.1

Eyring, V., Bock, L., Lauer, A., Righi, M., Schlund, M., Andela, B., et al. (2020). Earth System Model Evaluation Tool (ESMValTool) v2.0-an extended set of large-scale diagnostics for quasi-operational and comprehensive evaluation of Earth system models in CMIP. *Geoscientific Model Development*, *13*(7), 3383–3438.

Eyring, V., Bony, S., Meehl, G. A., Senior, C. A., Stevens, B., Stouffer, R. J., & Taylor, K. E. (2016a). Overview of the Coupled Model Intercomparison Project Phase 6 (CMIP6) experimental design and organization. *Geoscientific Model Development*, *9*(5), 1937–1958. https://doi.org/10.5194/gmd-9-1937-2016

Eyring, V., Cox, P. M., Flato, G. M., Gleckler, P. J., Abramowitz, G., Caldwell, P., et al. (2019). Taking climate model evaluation to the next level. *Nature Climate Change*, *9*(2), 102–110. https://doi.org/10.1038/s41558-018-0355-y

Eyring, V., Gleckler, P. J., Heinze, C., Stouffer, R. J., Taylor, K. E., Balaji, V., et al. (2016b). Towards improved and more routine Earth system model evaluation in CMIP. *Earth System Dynamics*, *7*(4), 813–830. https://doi.org/10.5194/esd-7-813-2016

Friedlingstein, P. (2001). Climate system and carbon cycle feedback. *Understanding the Earth System*, 163–177. https://doi.org/10.1007/978-3-642-56843-5_11

Friedlingstein, P., Bopp, L., Ciais, P., Dufresne, J. L., Fairhead, L., LeTreut, H., et al. (2001). Positive feedback between future climate change and the carbon cycle. *Geophysical Research Letters*, *28*(8), 1543–1546. https://doi.org/10.1029/2000GL012015

Friedlingstein, P., Cox, P., Betts, R., Bopp, L., Von Bloh, W., Brovkin, V., et al. (2006). Climate-carbon cycle feedback analysis: Results from the (CMIP)-M-4 model intercomparison. *Journal of Climate*, *19*(14), 3337–3353. https://doi.org/10.1175/jcli3800.1

Friedlingstein, P., Dufresne, J. L., Cox, P. M., & Rayner, P. (2003). How positive is the feedback between climate change and the carbon cycle? *Tellus Series B: Chemical and Physical Meteorology*, *55*(2), 692–700. https://doi.org/10.3402/tellusb.v55i2.16765

Friedlingstein, P., O'Sullivan, M., Jones, M. W., Andrew, R. M., Hauck, J., Olsen, A., et al. (2020). Global Carbon Budget 2020. *Earth System Science Data*, *12*(4), 3269–3340. https://doi.org/10.5194/essd-12-3269-2020

Gent, P. R., Danabasoglu, G., Donner, L. J., Holland, M. M., Hunke, E. C., Jayne, S. R., et al. (2011). The Community Climate System Model Version 4. *Journal of Climate*, *24*(19), 4973–4991. https://doi.org/10.1175/2011jcli4083.1

Gillett, N. P., Arora, V. K., Matthews, D., & Allen, M. R. (2013). Constraining the ratio of global warming to cumulative CO_2 emissions using CMIP5 simulations. *Journal of Climate*, *26*(18), 6844–6858. https://doi.org/10.1175/jcli-d-12-00476.1

Giorgetta, M. A., Jungclaus, J., Reick, C. H., Legutke, S., Bader, J., Böttinger, M., et al. (2013). Climate and carbon cycle changes from 1850 to 2100 in MPI-ESM simulations for the Coupled Model Intercomparison Project Phase 5. *Journal of Advances in Modeling Earth Systems*, *5*, 572–597. https://doi.org/10.1002/jame.20038

Gregory, J. M., Jones, C. D., Cadule, P., & Friedlingstein, P. (2009). Quantifying carbon cycle feedbacks. *Journal of Climate*, *22*(19), 5232–5250. https://doi.org/10.1175/2009jcli2949.1

Hajima, T., Tachiiri, K., Ito, A., & Kawamiya, M. (2014). Uncertainty of concentration-terrestrial carbon feedback in Earth system models. *Journal of Climate*, *27*(9), 3425–3445. https://doi.org/10.1175/jcli-d-13-00177.1

Jones, C. D., Arora, V., Friedlingstein, P., Bopp, L., Brovkin, V., Dunne, J., et al. (2016). C4MIP-The Coupled Climate-Carbon Cycle Model Intercomparison Project: Experimental protocol for CMIP6. *Geoscientific Model Development*, *9*(8), 2853–2880. https://doi.org/10.5194/gmd-9-2853-2016

Krinner, G., Viovy, N., de Noblet-Ducoudre, N., Ogee, J., Polcher, J., Friedlingstein, P., et al. (2005). A dynamic global vegetation model for studies of the coupled atmosphere-biosphere system. *Global Biogeochemical Cycles*, *19*, GB1015. https://doi.org/10.1029/2003GB002199

Lauer, A., Eyring, V., Bellprat, O., Bock, L., Gier, B. K., Hunter, A., et al. (2020). Earth System Model Evaluation Tool (ESMValTool) v2.0-diagnostics for emergent constraints and future projections from Earth system models in CMIP. *Geoscientific Model Development*, *13*(9), 4205–4228. https://doi.org/10.5194/gmd-13-4205-2020

Law, R. M., Ziehn, T., Matear, R. J., Lenton, A., Chamberlain, M. A., Stevens, L. E., et al. (2017). The carbon cycle in the Australian Community Climate and Earth System Simulator (ACCESS-ESM1)—Part 1: Model description and pre-industrial simulation. *Geoscientific Model Development*, *10*(7), 2567–2590. https://doi.org/10.5194/gmd-10-2567-2017

Lian, X., Piao, S., Huntingford, C., Li, Y., Zeng, Z., Wang, X., et al. (2018). Partitioning global land evapotranspiration using CMIP5 models constrained by observations. *Nature Climate Change*, *8*(7), 640–646. https://doi.org/10.1038/s41558-018-0207-9

Lindsay, K., Bonan, G. B., Doney, S. C., Hoffman, F. M., Lawrence, D. M., Long, M. C., et al. (2014). Preindustrial-control and twentieth-century carbon cycle experiments with the Earth System Model CESM1(BGC). *Journal of Climate*, *27*(24), 8981–9005. https://doi.org/10.1175/jcli-d-12-00565.1

Masson-Delmotte, V., Zhai, P., Pirani, A., Connors, S. L., Péan, C., Berger, S., et al. (2022). Climate Change 2021: The Physical Science Basis. Contribution of Working Group I to the Sixth Assessment Report of the Intergovernmental Panel on Climate Change.

Mauritsen, T., Bader, J., Becker, T., Behrens, J., Bittner, M., Brokopf, R., et al. (2019). Developments in the MPI-M Earth System Model version 1.2 (MPI-ESM1.2) and its response to increasing CO_2. *Journal of Advances in Modeling Earth Systems*, *11*, 998–1038. https://doi.org/10.1029/2018MS001400

Righi, M., Andela, B., Eyring, V., Lauer, A., Predoi, V., Schlund, M., et al. (2020). Earth System Model Evaluation Tool (ESMValTool) v2.0-technical overview. *Geoscientific Model Development*, *13*(3), 1179–1199. https://doi.org/10.5194/gmd-13-1179-2020

Schlund, M., Eyring, V., Camps-Valls, G., Friedlingstein, P., Gentine, P., & Reichstein, M. (2020a). Constraining uncertainty in projected Gross Primary Production with machine learning. *Journal of Geophysical Research: Biogeosciences*, *125*, e2019JG005619. https://doi.org/10.1029/2019JG005619

Schlund, M., Lauer, A., Gentine, P., Sherwood, S. C., & Eyring, V. (2020b). Emergent constraints on equilibrium climate sensitivity in CMIP5: Do they hold for CMIP6? *Earth System Dynamics*, *11*(4), 1233–1258. https://doi.org/10.5194/esd-11-1233-2020

Seland, O., Bentsen, M., Olivie, D., Toniazzo, T., Gjermundsen, A., Graff, L. S., et al. (2020). Overview of the Norwegian Earth System Model (NorESM2) and key climate response of CMIP6 DECK, historical, and scenario simulations. *Geoscientific Model Development*, *13*(12), 6165–6200. https://doi.org/10.5194/gmd-13-6165-2020

Sellar, A. A., Jones, C. G., Mulcahy, J. P., Tang, Y. M., Yool, A., Wiltshire, A., et al. (2019). UKESM1: Description and evaluation of the UK Earth System Model. *Journal of Advances in Modeling Earth Systems*, *11*, 4513–4558. https://doi.org/10.1029/2019MS001739

Swart, N. C., Cole, J. N. S., Kharin, V. V., Lazare, M., Scinocca, J. F., Gillett, N. P., et al. (2019). The Canadian Earth System Model version 5 (CanESM5.0.3). *Geoscientific Model Development*, *12*(11), 4823–4873. https://doi.org/10.5194/gmd-12-4823-2019

Taylor, K. E., Stouffer, R. J., & Meehl, G. A. (2012). An overview of CMIP5 and the experiment design. *Bulletin of the American Meteorological Society*, *93*(4), 485–498. https://doi.org/10.1175/bams-d-11-00094.1

Thornton, P. E., Lamarque, J.-F., Rosenbloom, N. A., & Mahowald, N. M. (2007). Influence of carbon-nitrogen cycle coupling on land model response to CO_2 fertilization and climate variability. *Global Biogeochemical Cycles*, *21*, GB4018. https://doi.org/10.1029/2006GB002868

Tjiputra, J. F., Roelandt, C., Bentsen, M., Lawrence, D. M., Lorentzen, T., Schwinger, J., et al. (2013). Evaluation of the carbon cycle components in the Norwegian Earth System Model (NorESM). *Geoscientific Model Development*, *6*(2), 301–325. https://doi.org/10.5194/gmd-6-301-2013

Watanabe, S., Hajima, T., Sudo, K., Nagashima, T., Takemura, T., Okajima, H., et al. (2011). MIROC-ESM 2010: Model description and basic results of CMIP5-20c3m experiments. *Geoscientific Model Development*, *4*(4), 845–872. https://doi.org/10.5194/gmd-4-845-2011

Weigel, K., Bock, L., Gier, B. K., Lauer, A., Righi, M., Schlund, M., et al. (2021). Earth System Model Evaluation Tool (ESMValTool) v2.0— Diagnostics for extreme events, regional and impact evaluation, and analysis of Earth system models in CMIP. *Geoscientific Model Development*, *14*(6), 3159–3184. https://doi.org/10.5194/gmd-14-3159-2021

Wenzel, S., Cox, P. M., Eyring, V., & Friedlingstein, P. (2014). Emergent constraints on climate-carbon cycle feedbacks in the CMIP5 Earth system models. *Journal of Geophysical Research: Biogeosciences*, *119*, 794–807. https://doi.org/10.1002/2013JG002591

Wenzel, S., Cox, P. M., Eyring, V., & Friedlingstein, P. (2016). Projected land photosynthesis constrained by changes in the seasonal cycle of atmospheric CO_2. *Nature*, *538*(7626), 499–501. https://doi.org/10.1038/nature19772

Yukimoto, S., Kawai, H., Koshiro, T., Oshima, N., Yoshida, K., Urakawa, S., et al. (2019). The Meteorological Research Institute Earth System Model Version 2.0, MRI-ESM2.0: Description and basic evaluation of the physical component. *Journal of the Meteorological Society of Japan*, *97*(5), 931–965. https://doi.org/10.2151/jmsj.2019-051

Zaehle, S., Friedlingstein, P., & Friend, A. D. (2010). Terrestrial nitrogen feedbacks may accelerate future climate change. *Geophysical Research Letters*, *37*, L01401. https://doi.org/10.1029/2009GL041345

Zickfeld, K., Eby, M., Matthews, H. D., Schmittner, A., & Weaver, A. J. (2011). Nonlinearity of carbon cycle feedbacks. *Journal of Climate*, *24*(16), 4255–4275. https://doi.org/10.1175/2011jcli3898.1

Ziehn, T., Lenton, A., Law, R. M., Matear, R. J., & Chamberlain, M. A. (2017). The carbon cycle in the Australian Community Climate and Earth System Simulator (ACCESS-ESM1)—Part 2: Historical simulations. *Geoscientific Model Development*, *10*(7), 2591–2614. https://doi.org/10.5194/gmd-10-2591-2017